1 **Leaching behaviour of co-disposed steel making wastes: Effects of aeration**
2 **on leachate chemistry and vanadium mobilisation**

3

4 **Andrew J. Hobson[a], Douglas I. Stewart[b], Robert J. G. Mortimer[c], William M. Mayes[d],**
5 **Mike Rogerson[d] and Ian T. Burke[a*]**

6

7 [a]School of Earth and Environment, University of Leeds, Leeds, LS2 9JT, UK.
8 *Corresponding Author's E-mail: i.t.burke@leeds.ac.uk Phone: +44 113 3437532; Fax: +44
9 113 3435259

10 [b]School of Civil Engineering, University of Leeds, Leeds, LS2 9JT, UK.

11 [c]School of Animal, Rural and Environmental Sciences, Nottingham Trent University,
12 Brackenhurst Campus, Southwell, Nottinghamshire NG25 0QF

13 [d]School of Environmental Sciences, University of Hull, Hull, HU6 7RX, UK.

14

15

16

17

19

20 **Highlights**

21 • Steel making by-products unsuitable for recycling stored in landfill
22 • Leaching mechanism is primarily controlled by air availability
23 • Air-exclusion led to Ca-rich, high pH leachates, with low V concentrations
24 • Carbonate formation during aeration led to lower pH but higher V concentrations

25

26   **Abstract**

27   Steelmaking wastes stored in landfill, such as slag and spent refractory liners, are often

28   enriched in toxic trace metals (including V). These may become mobile in highly alkaline

29   leachate generated during weathering. Fresh steelmaking waste was characterised using XRD,

30   XRF, and SEM-EDX. Batch leaching tests were performed under aerated, air-excluded and

31   acidified conditions to determine the impact of atmospheric CO_2 and acid addition on leachate

32   chemistry. Phases commonly associated with slag including dicalcium silicate, dicalcium

33   aluminoferrite, a wüstite-like solid solution and free lime were identified, as well as a second

34   group of phases including periclase, corundum and graphite which are representative of

35   refractory liners. During air-excluded leaching, dissolution of free lime and dicalcium silicate

36   results in a high pH, high Ca leachate in which the V concentration is low due to the constraint

37   imposed by $Ca_3(VO_4)_2$ solubility limits. Under aerated conditions, carbonation lowers the

38   leachate pH and provides a sink for aqueous Ca, allowing higher concentrations of V to

39   accumulate. Below pH 10, leachate is dominated by periclase dissolution and secondary phases

40   including monohydrocalcite and dolomite are precipitated. Storage of waste under saturated

41   conditions that exclude atmospheric CO_2 would therefore provide the optimal environment to

42   minimise V leaching during weathering.

43

1   Introduction

Steel slag is a ubiquitous byproduct of the steelmaking industry that is produced in large

quantities worldwide. It is estimated that 160-240 million tonnes of steel slag were produced

in 2016 (Ober, 2017) which corresponds to approximately 10-15 % of crude steel output

(Piatak et al., 2014). Primary steelmaking (i.e. conversion of iron to steel) produces steel slag

via two principal production methods; 1) basic oxygen furnace (BOF) steelmaking in which

molten iron from a blast furnace is used and 2) electric arc furnace (EAF) steelmaking which

uses a combination of scrap steel, directly reduced iron and pig iron. In both processes lime (or

limestone) is added to the furnace as a fluxing agent to remove impurities from the molten

metal (Eloneva et al., 2010, Piatak et al., 2014). The composition of BOF and EAF slag is

broadly similar and consistent across location and process (Tossavainen et al., 2007, Yildirim

and Prezzi, 2011, Proctor et al., 2000). These predominantly consist of Ca, Mg, Fe and Al

oxides and silicates (Proctor et al., 2000); the relative proportions of which will vary according

to the raw materials used during manufacture. Secondary steelmaking slags are formed during

secondary steelmaking where both BOF and EAF derived steels are further processed in ladle

furnaces, producing BOF(L) or EAF(L) slags respectively. These are much more variable in

composition and are also relatively enriched in Mg and Al due to additives used in the process

(Shi, 2002). In addition to slag production, a wide variety of refractories (MgO-C; Al-silicate;

$MgO-Al_2O_3-C$) are used as furnace liners during steelmaking to protect the furnace (Quaranta

et al., 2014). Refractories that are in contact with molten slag wear over time and the build-up

of solidified slag above the melt (due to sputtering) and in conduits also require regular

removal. Therefore, periodic renewal of the entire liner is required. The result is a mixed waste

containing both slag and refractories which is difficult to separate and are often co-disposed

(Hanagiri et al., 2008).

68   Primary steelmaking slags are recycled where possible, usually as aggregate in civil

69   engineering applications, such as road construction and as a general fill material due to its

70   stability (Geiseler, 1996, Yi et al., 2012). However, in some cases elevated concentrations of

71   free lime (CaO) and periclase (MgO), which expand on hydration, preclude reuse in

72   engineering applications. Ladle slags and refractories can also be recycled during primary

73   steelmaking (as an alternative source of CaO or MgO flux) but virgin materials are often

74   preferred due to their more uniform composition and the increased effort that would be required

75   in slag sorting and processing (Kwong and Bennett, 2002, de Sa et al., 2007). For this reason,

76   and also because supply frequently exceeds the demand for secondary aggregates, steelmaking

77   byproducts are often stored either in landfill or in open 'heaps'. However, as recycling rates

78   increase, materials with problematic properties (e.g. high metal content, high % of CaO or

79   MgO, or simply uncertain or variable composition) will make up an ever greater proportion of

80   materials stored in landfill. It is therefore increasingly import to understand the leaching

81   behaviour of such non-standard by-products as they become a significant part of the disposed

82   inventory.

83   Steel slags contain free lime (CaO) and periclase (MgO; also in present in refractories)

84   that hydrate to form portlandite ($Ca(OH)_2$) or brucite ($Mg(OH)_2$). These phases dissolve in

85   water to generate high pH (10.5-12.5) leachate (Mayes et al., 2008):

86    $$CaO_{(s)} + H_2O \rightarrow Ca(OH)_{2(aq)} \rightleftharpoons Ca^{2+} + 2OH^- \qquad pH_{(eq.)} = 12.46 \text{ (1)}$$

87    $$MgO + H_2O \rightarrow Mg(OH)_{2(aq)} \rightleftharpoons Mg^{2+} + 2OH^- \qquad pH_{(eq.)} = 10.40 \text{ (2)}$$
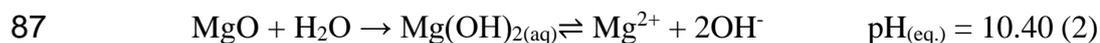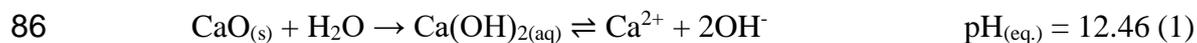
88   Alkalinity may also be produced by the dissolution of Ca-silicates, (e.g. β-dicalcium silicate,

89   larnite; Roadcap et al. (2005)):

90    $$Ca_2SiO_4 + 2H_2O \rightarrow 2Ca^{2+} + H_2SiO_4^{2-} + 2OH^- \qquad\qquad \text{(3)}$$

5

91   In addition, under aerated conditions, reactions involving the in-gassing of CO_2 results in

92   conversion of Ca/Mg hydroxide based alkalinity to carbonate alkalinity.

93        $$Ca^{2+}_{(aq)} + CO_{2(aq)} + 2OH^-_{(aq)} \rightarrow CaCO_{3(s)} + H_2O_{(l)} \tag{4}$$

94        $$CaCO_3 + H_2O \rightleftharpoons Ca^{2+} + HCO_3^- + OH^- \qquad pH_{(eq.)} = 9.36 \tag{5}$$
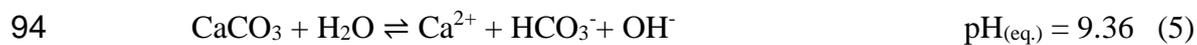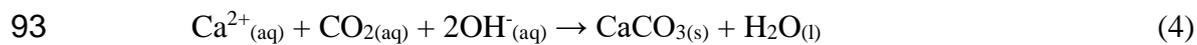
95   Whilst steel slag has historically been considered to be a non-hazardous waste, concerns

96   have been raised in recent years regarding the high concentrations of potential toxic trace

97   metal(loid)s (including Al, Cr, Pb, Mo and V) present in the slag (Tossavainen et al., 2007,

98   Proctor et al., 2000, Matern et al., 2013) which may be mobilised in the alkaline leachate

99   (Cornelis et al., 2008). V leaching in particular has received a lot of recent attention (Chaurand

100   et al., 2006, De Windt et al., 2011, Huijgen and Comans, 2006, Navarro et al., 2010) due to its

101   relative enrichment in steel slags and regulatory concern over high V concentrations in

102   leachates (Environment Agency, 2014). Steelmaking wastes at disposal sites are often

103   deposited in both saturated and unsaturated settings, however, few data currently exist

104   concerning slag leachate generation and chemistry under aerated conditions (Bayless and

105   Schulz, 2003, Roadcap et al., 2005, Mayes and Younger, 2006). Under aerated conditions,

106   $CaCO_3$ precipitation results in a drop in solution pH as OH^- ions are consumed (equation 4).

107   Changes in both pH and redox have significant implications for the mobility of many

108   potentially toxic metals; for example Al, Cr , and V mobility and toxicity are all highly

109   dependent on their speciation (with higher oxidation states generally regarded as more toxic

110   and mobile) (Pourbaix, 1966).

111   This study investigates leaching behaviour of co-disposed steelmaking waste under

112   aerated and air-excluded conditions. These represent contrasting conditions present either near

113   the surface (good contact with atmosphere) and below the water table deeper within waste

114   heaps. The waste has been characterised using x-ray diffraction (XRD) and fluorescence (XRF)

115 techniques, as well as scanning electron microscopy (SEM) with energy-dispersive x-ray

116 spectroscopy (EDX) to determine the mineral phases present. Fully aerated and air-excluded

117 water leaching tests have been performed to determine how phase dissolution behaviour,

118 secondary mineral formation and trace metal release are affected by changes in pH and

119 availability of air. Results will assist prediction of metal release from waste when stored in

120 landfill above and below the water table, enabling effective environmental risk assessment and

121 cost-effective long-term management of the waste.

2   Methods and Materials

2.1   Sample collection and characterisation

Samples were collected within one week of deposition from the Yarborough Landfill (British Steel, Scunthorpe, UK) in May 2013 (LAT 53°35′22.24″ LONG 0°35′41.52″). The sample consisted of 50-500 g blocks (~100 kg total). A sub-sample of the collected material (approx. 500 g consisting of 50 g pieces) were brushed to remove any fines and crushed to provide a homogenised powder consisting of 20-100 μm particles. The crushed waste was stored in a polythene bag within an airtight glass jar containing soda lime to prevent weathering due to contact with atmospheric CO_2 and moisture.

Elemental analysis of the powdered waste was undertaken using a PANalytical Axios Advanced X-ray Fluorescence (XRF) spectrometer (data corrected for loss on ignition at 1050 °C). Samples were prepared for major element analysis as fused beads with lithium metaborate/tetraborate flux (Johnson Matthey Spectroflux JM100B) (0.6 g sample; 3 g flux). For minor/trace element analysis pressed pellets were prepared containing ~10 g of dried waste using ~10–20 drops of 6.6 % w/v polyvinyl alcohol in a 1:6 mix of methanol and distilled deionized water as a binder (Moviol 88 solution). The elemental limit of detection (LoD) was generally < 0.02 wt% and the analytical uncertainty (versus certified reference standards) was $< \pm10\%$ of the data value. Mineralogical analysis (LoD was approximately 3 wt% for crystalline phases) was undertaken by powder X-ray diffraction (XRD) using a Bruker D8 diffractometer, where powder samples were mounted on silicon slides and scanned between 2° and 70° 2θ using Cu K_{α} radiation. Diffraction peaks from unknown samples were then matched to known standard reference patterns using Diffrac.Suite Eva v3.0 software using the International Centre for Diffraction Data (ICDD) PDF2 database (powder diffraction file (PDF) reference numbers are reported for identified phases).

146   Two polished blocks were prepared by first cutting waste pieces to size under water

147   and setting the resultant ~2 cm^3 blocks into epoxy resin with the cut surface exposed. This

148   surface was then polished using a water-free diamond paste to remove the top 1-2 mm of

149   material potentially exposed to water during cutting. Electron micrographs were subsequently

150   collected on a FEI QUANTA 650 FEG ESEM, which was equipped for Oxford Instruments

151   INCA 350 energy-dispersive X-ray spectroscopy (EDS) system/80 mm X-Max silicon drift

152   detector. EDS spectra and elemental maps were collected and analysed using Oxford

153   Instruments AZtec software. The element and sample specific LoD for EDS analysis was

154   between 0.1 and 0.5 wt%.

155   2.2   Acid Neutralisation Capacity (ANC)

156   Homogenised powdered waste (0.4 g) was mixed with 40 mL HCl with concentrations

157   ranging from 1 M to 0.001 M in 50 mL polypropylene Oak Ridge tubes (Nalgene, USA).

158   Experiments were performed in triplicate. Headspaces of the 50 ml tubes were flushed with N_2

159   gas prior to sealing. All tubes were subsequently stored in airtight 2 L glass jars (Le Parfait,

160   France) filled with N_2 gas and also containing ~100 g soda lime (as a CO_2 absorbent) to prevent

161   any CO_2 infiltration from atmosphere to the experimental tubes. After 1 and 50 days

162   equilibration the 50 ml tubes were centrifuged in a Sigma 2-16 centrifuge using a 12151 rotor

163   at 8000 rpm (6000 g) for 5 minutes to separate aqueous and solid phases. 1 mL of the

164   supernatant was removed and immediately added to 9 mL 0.1 M HNO_3 prior to ICP analysis,

165   and the pH of the remaining solution was measured (pH measurement is described below).

166   2.3   Leaching tests

167   Triplicate aerated experiments containing 1 g homogenised powdered waste and 100

168   mL deionised water were established in open 500 mL PETG Erlenmeyer flasks. These were

169   gently agitated on a Stuart Scientific SSL1 orbital shaker at 175 rpm to allow for equilibrium

170   of the reaction solution with air (i.e. dissolution of atmospheric CO_2 and O_2). At regular

171   intervals over a 50 day period 3 mL aliquots of slurry were removed from the flasks and

172   centrifuged in 2 x 1.5 ml Eppendorf tubes in a Spectrafuge 16M microcentrifuge at 14,000 rpm

173   (16,000 g) for 5 minutes to separate aqueous and solid phases. 1 mL of supernatant was

174   removed and acidified in 0.1 M HNO_3 and the pH of the remaining supernatant was determined.

175   The moist solid samples were stored at -20 °C prior to drying at 40 °C overnight for further

176   analysis.

177   Replicate air-excluded experiments were established containing 0.4 g homogenised

178   powdered waste and 40 mL deionised water in 50 mL Oak ridge tubes. All tubes were

179   anaerobically handled as described above for the ANC tests. Periodically over a 50 day period

180   3 tubes were sacrificially sampled. Solid and solution samples were taken and stored following

181   the procedures above.

182   2.4   Aqueous Analysis

183   Solution pH (±0.2 pH units) was measured using an Orion DualStar pH/ISE benchtop

184   meter (Thermo Scientific, USA) with an electrode that was calibrated daily at pH 4, 7 and 10.

185   Nitrogen gas was bubbled through the sample tube during pH measurements made in solutions

186   from the air-excluded experiments to prevent contact with atmosphere. Metal concentrations

187   in acidified aqueous samples from the air-excluded leaching experiments were determined

188   (with an analytical uncertainty of $< \pm 3\%$) using a Thermo iCAP 7400 ICP-OES ion-coupled

189   plasma, optical emission spectrometer (ICP-OES; for Ca, Si, Mg; LoDs were $< 10 \, \mu g \, L^{-1}$) and

190   Thermo iCAP Qc ion-coupled plasma, mass spectrometer (ICP-MS; for V, Mn, and Cr with

191   LoDs $< 0.1 \, \mu g \, L^{-1}$; for Li and Fe with LoD $< 2 \, \mu g \, L^{-1}$). Calibration was against certified multi-

192   element standards and check samples were analysed every 10 samples to check for calibration

193   drift. Aqueous elemental concentrations from the aerated leaching experiments were

194   determined using a Perkin Elmer Optima 5300DV ICP-OES for all elements (LoDs were < 100

195   µg L^{-1} for all elements). The 5300DV was calibrated with 3 standards (0.1, 1, 10 mg L^{-1}) and a

196   blank which were run every 15 samples and the calibration cross-checked with a trace metal

197   Certified Reference Material (NIST1646A) with all values within ±5%.

198

3 **Results**

200 3.1 Material Characterisation

201 The elemental composition (Table 1) of the powder sample was dominated by Ca, Fe,

202 Mg, Si and Al with Cr and Mn as minor constituents. Trace elements included P, V, K, Ti

203 and S.

204 [TABLE 1]

205 Mineralogical analysis of the crushed waste using XRD (Fig. 1a) identified the presence

206 of periclase (MgO; PDF #44-946), corundum (Al_2O_3; PDF #10-173), larnite (dicalcium

207 silicate, β-Ca_2SiO_4; PDF #33-302), brownmillerite (dicalcium aluminoferrite, $Ca_2(Al,Fe)_2O_5$;

208 PDF #30-226), wüstite (FeO; PDF #46-1312), brucite ($Mg(OH)_2$; PDF #44-1482) and

209 elemental carbon (graphite-C; PDF #23-64). The principal XRD peak of free lime (CaO; PDF

210 #37-1497) overlaps with a secondary peak of corundum at ~37.5° 2θ, however, the secondary

211 peaks at ~ 32 and 54 ° 2θ were present, suggesting its presence. There was no calcite peaks in

212 the XRD pattern for the unreacted waste (n.b. the principle calcite peak is at ~29 ° 2θ).

213 [FIGURE 1]

214 SEM analysis of a polished block (Fig. 2) showed a material that was composed of

215 intergrown 10-30 µm crystallites, EDS elemental mapping indicated that there were three

216 dominant compositions. The dominant composition by area (~ 65 % of the sample viewed) was

217 a Ca-Si-O rich phase containing trace amounts of Al, P, Ti, V and Fe by EDS analysis,

218 consistent with the larnite phase identified by XRD. The second most abundant composition

219 by area (~25 %) was a Mg-Fe-O rich phase containing trace amounts of Na, Ca, Cr and Mn,

220 corresponding to the wüstite phase identified by XRD. The third most abundant composition

221 by area (~10 %) was a Ca-Fe-Al-O rich phase containing trace amounts of Ti, V, Cr and Mn,

222 corresponding to the brownmillerite phase identified by XRD. Regions of the dicalcium silicate

223 phase contain lamellae identified as CaO rich regions associated with dicalcium silicate. The

224 second polished block was composed of a single Al-Si-O rich composition containing no

225 significant trace elements (data not shown).

226   [FIGURE 2]

227 3.2   Acid Neutralisation Tests.

228   For crushed waste, the relationship between the final solution pH value and the amount

229 of acid added was similar after 1 day and 50 days of equilibration (Fig. 3a). The acid

230 neutralisation capacity (to pH 7) was very similar at the two time-points (11.0 and 9.5 M H^+

231 kg^{-1} waste, respectively). In tests where the final pH value was greater than 7, the pH value

232 increased with time. The solution Ca and Mg concentrations at a particular pH value were

233 broadly similar after 1 day and 50 days (Fig. 3c, d), however, Si (Fig. 3b) was present in

234 solution at all final pH values < 10 after 1 day, but was present at significantly reduced

235 concentrations at 50 days at all pH values. Calcium was released to solution at all pH values,

236 with generally higher concentrations at lower pH values. Magnesium was only present in

237 solution below ~pH 10, but also has generally higher concentrations at lower pH values.

238   [FIGURE 3]

239 3.3   Batch leaching tests

240   During air-excluded leaching (Fig. 4), the leachate pH rose rapidly within the first hour

241 to a value of 11.4, and then increased more slowly to a maximum value of 11.9 after 52 days.

242 The Ca concentration increased rapidly to ~2.5 mmol L^{-1} over the first 24 hrs, and then more

243 steadily to ~3.0 mmol L^{-1} after 5 days. Between 5 days and 10 days the Ca concentration

244 decreased to ~2.5 mmol L^{-1}, but thereafter increased steadily to ~3.4 mmol L^{-1} after 50 days.

245 The Mg concentration showed no trend with time and was less than 0.4 mmol L^{-1} throughout

246 the experiment. The Si concentration increased to ~0.15 mmol L^{-1} over the first 24 hrs, and

13

247   then to ~0.25 mmol L^{-1} after 5 days. After about 10 days the Si concentration decreased to

248   ~0.15 mmol L^{-1} but subsequently varied between ~0.15 and ~0.25 mmol L^{-1} until the end of

249   the test. The V concentration gradually increased from ~0.002 mmol L^{-1} after 24hrs to ~0.007

250   mmol L^{-1} after 50 days. Aqueous Fe concentrations range from 0.002 to 0.07 mmol $L^{-1}$and

251   were just above the limit of detection by ICP-MS (0.0018 mmol L-1), which increases scatter

252   in the data. However is still discernible that Fe accumulated in solution during the air-excluded

253   experiments and did not in parallel aerated experiments. There was very little change in XRD

254   patterns collected from the solid residue over time, except that portlandite (PDF #44-1481) was

255   detected in samples collected from the experiment end points (Fig 1b).

256   [FIGURE 4]

257   During the aerated experiments (Fig. 4), pH increased rapidly within the first hour to a

258   maximum value of 11.6. This was followed by a decrease to pH 8.9 after 1 day and then by a

259   second rise to pH 10.0 after 6 days. Subsequently pH steadily declined to 9.3 after 50 days of

260   leaching. The Ca concentration increased rapidly to ~2 mmol L^{-1} within the first two hours, but

261   then decreased to ~0.25 mmol L^{-1} after 6-7 days. Initially the Mg concentration was low but it

262   increased rapidly after day 2 to reach a concentration above 12.5 mmol L^{-1} by day 20, which

263   persisted until the end of the test. The Si concentration was ~0.15 mmol L^{-1} after 1 hour,

264   decreased to ~0.03 mmol L^{-1} after 2 days but then rose to ~0.25 mmol L^{-1} at 6 days.

265   Subsequently Si concentrations remained above 0.2 mmol L^{-1} for the remainder of the test. The

266   V concentration increased steadily over the duration of the test to reach a maximum of ~0.065

267   mmol L^{-1} after 48 days. The aqueous Fe concentrations were initially around 0.05 mmol L^{-1}

268   and decreased over 5 days to < 0.002 mmol L^{-1} for the remainder of the tests. XRD patterns

269   collected from solid residue after 1 day show that calcite (PDF #24-27) was present (Fig. 1c),

270   after 6 days the periclase and larnite peaks had reduced in relative intensity and

271   monohydrocalcite (PDF #29-306) was detected (Fig 1d). After 50 days monohydrocalcite was

14

272 the dominant secondary phase detected (although some dolomite, PDF #36-426, was also

273 present) and periclase and larnite peaks were absent (Fig. 1e).

274   Concentrations of other trace elements considered to be potential environmental risk

275 drivers for steel slags (e.g. Mn, Cr, Li) were low in both the aerated and the air-excluded tests

276 (and were present at concentrations close to or below to the limit of detection).

277

278 **4** **Discussion**

279 4.1 Waste characterisation

280 The bulk chemical and mineralogical composition of the waste was distinct from BOF

281 slag samples collected at the Yarborough site (Table 1). Compared to BOF slag the material

282 was relatively depleted in elements such as Ca, Fe, Mn and V; but enriched in Mg, Al, Ti and

283 Cr. The waste mineralogy could be split into two distinct groups. The first group included a

284 range of phases commonly occurring in BOF slag (i.e. larnite, brownmillerite, lime, and

285 wüstite; Yildirim and Prezzi (2011), Proctor et al. (2000), Geiseler (1996)), which were

286 observed in SEM as discrete particle assemblages within an intergrown matrix of 20-50 µm

287 crystallites. The second group of minerals identified by XRD included corundum, periclase

288 and graphite that are rare in BOF slag and are more commonly associated with refractory liner

289 materials (e.g. in MgO-C and AL_2O_3-MgO-C refractories; Rovnushkin et al. (2005)).

290 Aluminosillicate was also observed in SEM analysis. This was most likely the high temperature

291 phase mullite ($Al_6Si_2O_{13}$; Schneider et al. (1994), Chesters (1973), Mazdiyasni and Brown

292 (1972), Tamari et al. (1993)) which is also used as a refractory material or can form in slags

293 from reaction of corundum and Si (Dana and Das, 2004, Zhao et al., 2014). Therefore, the

294 waste can be characterised as a mixed steelmaking waste containing both BOF slag and

295 refractory materials. The potential for re-use of mixed wastes is low due to uncertainties about

296 their chemical and physical behaviour, however, it is important to understand their potential

297 leaching behaviour during disposal.

298

299 4.2 Acid neutralisation behaviour

300 The acid neutralisation capacity experiments were conducted under air-excluded

301 conditions and provide information on phase dissolution in the waste as a function of the acid

302   addition and final solution pH. At low acid additions (< 1 mol H^+ kg^{-1}) the waste buffered pH

303   to values > 11.5 due to the dissolution of free lime and dicalcium silicate (Eqns. 1 and 3), with

304   dissolution of brucite from periclase hydration also consuming acid when the pH < 10.4 (Eqn.

305   2). Ca was released to solution at all pH values with the amount of release increasing with

306   decreasing pH (Fig. 3c), and Mg was released to solution when pH values < 10 with the amount

307   of release also increasing with decreasing pH (Fig. 3d), which is consistent with the dissolution

308   behaviour of these phases (Eqns 1 and 2). The alkalinity producing phases were progressively

309   exhausted by larger acid additions and the final pH decreased steadily until neutral values were

310   reached with an acid addition of ~8 mols H^+ kg^{-1}. CaO hydration is a very fast reaction (Shi et

311   al., 2002), whereas dicalcium silicate hydration and dissolution is generally considered to be

312   slower (Taylor, 1986). However, here we find that both are involved in buffering the pH in the

313   first 24 hrs as Si is released to solution. Nevertheless, the 10:1 ratio in the aqueous Ca and Si

314   concentrations indicated an excess of Ca release relative to pure dicalcium silicate dissolution

315   (i.e. Ca : Si $\approx$ 2:1) suggesting that free lime was the dominant Ca bearing phase that was

316   dissolving over 24 hrs.

317   The difference in the final pH of the 1 and 50 day tests with the same acid addition

318   indicates that part of the alkalinity generation occurs over longer time periods. At high pH this

319   was most likely associated with continued dissolution of dicalcium silicate, although the Si

320   concentrations decreased between day 1 and 50. This Si decrease was most likely associated

321   with the formation of secondary Si-containing phases. These phases were most probably

322   calcium-silicate-hydrate (Ca-Si-H) phases at pH values > 9 (Walker et al., 2016, Costa et al.,

323   2016) and amorphous silica ($SiO_{2\ (am)}$) at lower pH values (Langmuir, 1997). The increase in

324   Mg concentration between day 1 and 50 at pH values < 9 suggests periclase hydration also

325   continued beyond 24 hours.

326

327   4.3   Leaching behaviour under aerated conditions

328   At the initial sampling point (1 hr) during the aerated leaching tests, the pH value was

329   11.5 ±0.2 and both Ca and Si were released to solution. This rapid initial release of alkalinity,

330   Ca and Si was due to the hydration and dissolution of both free lime and dicalcium silicate

331   phases present in the waste. Previous slag leaching tests using granulated BOF slag pieces

332   found dicalcium silicate dissolution to be significantly slower than free lime dissolution

333   (Stewart et al., 2018). The use of crushed powder samples in these tests which will have

334   contained high surface area fines must have promoted rapid initial dissolution of dicalcium

335   silicate. However, as dicalcium silicate dissolution releases Ca and Si to solution in an

336   approximately 2:1 ratio (Hobson et al., 2017), the much higher initial Ca/Si ratios in solution

337   (between 13 and 20) indicates that free lime dissolution was most likely to be the predominant

338   source of rapidly leached alkalinity in these tests.

339   In the 2 days after the initial release of alkalinity Ca and Si to solution, the pH reduced

340   to 8.9 contemporaneously with rapid Ca and Si removal. The decrease in pH and Ca

341   concentrations coincides with the appearance of calcite peaks in the XRD plots after 1 hour

342   (Fig. 1) indicating that the initial spike in pH was buffered down to 8.9 due to in-gassing of

343   atmospheric CO_2 and the subsequent precipitation of $CaCO_3$, which consumes both OH^- and

344   Ca^{2+} ions (Eqn. 4). The contemporaneous decrease in Si concentrations may be evidence of the

345   formation of a calcium silicate hydrate phase (Ca-Si-H). Indeed, low Ca/Si ratio (< 1) Ca-Si-H

346   phases are predicted to form under the observed initial pH and Ca concentrations on a timescale

347   of 24-48 hours (Walker et al., 2016). The peaks associated with dicalcium silicate (larnite) in

348   XRD patterns became less prominent over time and were ultimately absent by the end of the

349   experiments, indicating continued dicalcium silicate dissolution beyond day 6. Despite this no

350   further increase in Ca concentration was observed after 2 days, probably because most of the

351   Ca released by dicalcium silicate dissolution was precipitated as $CaCO_3$ under aerated

352   conditions (monohydrocalcite peaks became increasingly prominent in the XRD pattern over

353   time). Si concentration increased to a maximum value between 2-6 days contemporaneously

354   with a second observed peak in pH. There are only modest changes in Si concentrations

355   observed after 6 days, suggesting that equilibrium with secondary Si-containing phases such

356   as Ca-Si-H or amorphous SiO_2 (Langmuir, 1997, Costa et al., 2016, De Windt et al., 2011) was

357   limiting Si concentrations in these experiments.

358   XRD analysis indicates that there was progressive loss of periclase from the solids over

359   time, such that it was absent from the final XRD pattern. There were also small brucite peaks

360   in the XRD patterns from all time points. Periclase hydrates in water to form brucite

361     $(Mg(OH)_2)$, which readily dissolves at pH values < 10.4 (Eqn. 2). No significant Mg release to

362   solution was observed during the first 24 hours of leaching because brucite is relatively

363   insoluble at the then prevailing high pH value that was imposed by CaO and calcium silicate

364   weathering. After the initial spike in the pH value on the first day, the solution pH was lower

365   than the brucite equilibrium value, and the aqueous Mg concentration increased as brucite

366   dissolved. As a result, periclase hydration and brucite dissolution provided an additional source

367   of alkalinity to the system. Dissolution of brucite leads to a switch in solution chemistry from

368   a Ca to an Mg dominated system. Monohydrocalcite was observed in XRD patterns after day

369   6, after which it becomes the dominant carbonate phase, demonstrating a switch from calcite

370   formation in the Mg-free early part of the experiments to predominately monohydrocalcite

371   formation in the Mg-dominated system present after day 6. Recent studies have shown that an

372   Mg-rich environment, such as that observed after 5 days, may support the precipitation of

373   monohydrocalcite $(CaCO_3 \cdot H_2O)$ into which Mg may be incorporated (Rodriguez-Blanco et al.,

374   2014). At later time points dolomite $(CaMg(CO_3)_2)$ was detected in XRD analysis, which may

375   also form due to the high Mg concentrations suppressing calcite or aragonite formation during

376   recrystallisation of monohydrocalcite (Rodriguez-Blanco et al., 2014).

378   4.4   Leaching behaviour under air-excluded conditions

379   At the first sampling point at 1 hr the pH value and the Ca and Si concentrations were

380 very similar to those observed in the aerated experiments (pH 11.5 ±0.2, [Ca] 1.5 ±0.5 mmol

381 L-1 and [Si] 0.15 ±0.025 mmol L-1) indicating similar processes were occurring over the first

382 hour of leaching in both experiments (i.e. rapid dissolution of free lime and fine grained

383 dicalcium silicate particles). As a saturated $Ca(OH)_2$ solution will reach a pH of ~12.5 (Eqn. 1)

384 and experimental pH values were between 11 and 12 at all-time points, it suggests that the

385 magnitude of the initial rise in pH was mass limited (i.e. controlled by the amounts of CaO and

386 reactive dicalcium silicate that are readily available for dissolution) rather than $Ca(OH)_2$

387 solubility limited. Between the first sampling point and day 5 there was a slow increase in pH,

388 Ca and Si which was probably the result of continued dicalcium silicate dissolution.

389   Between day 5 and 10 in the air-excluded experiments there was a decrease in Ca

390 concentrations that coincided with a decrease in Si concentrations, which suggests that a Ca-

391 Si-H phase formed. The pH, Ca and Si concentrations present at the time of formation in the

392 leaching experiments were consistent with precipitation of a Ca-Si-H phase with Ca/Si ratio of

393 close to 1 (Walker et al., 2016). The continuing slow rise in pH, Ca and Si concentrations

394 during the remainder of the experiment indicate that under air-excluded conditions, the solution

395 composition slowly evolves towards dicalcium silicate solubility limits over time (also

396 observed by De Windt et al. (2011)). However, Ca-Si-H gel formation can cover particle

397 surfaces, making alkalinity generation a diffusion-limited process (Hobson et al., 2017, Costa

398 et al., 2016, Nikolić et al., 2016), slowing the dissolution of the remaining reactive solid phases,

399 and leading to the incomplete dissolution of larnite (dicalcium silicate) observed at the end of

400 these experiments (Fig. 1b). No Mg was released to solution under air-excluded conditions

401 because the pH remained above 10.4 throughout the experiments, and therefore, dissolution of

402 the Mg containing phases was inhibited.

403

404 4.5   Control of trace metal release

405   Fe can be released to solution during dissolution of both free lime and dicalcium silicate

406 (in which it can be a minor constituent; Hobson et al. (2017)), and therefore Fe is present in the

407 leachate throughout the air-excluded experiments (The slightly lower Fe concentrations after 5

408 days under air-excluded conditions may be due in part to incorporation of some Fe into Ca-Si-

409 H phases). Conversely, under aerated conditions Fe is only present in significant concentrations

410 during the first 3 days during which time the leachate pH falls from 11.5 to 9. Under aerated

411 conditions, any Fe(II) released is likely to be readily oxidised to Fe(III) and precipitated either

412 as an insoluble hydroxide or incorporated into spinel-like secondary phases (e.g. magnetite,

413 Fe_3O_4: De Windt et al. (2011)) at pH 9, limiting Fe accumulation in solution.

414   Vanadium release in the air-excluded experiments is low (maximum of ~0.007 mmol

415 L^{-1}) compared to that observed in the aerated experiments (maximum of ~0.065 mmol L^{-1}).

416 Previous work on BOF slag weathering suggests that it is V(V) associated with dicalcium

417 silicate which is most readily leached to solution (Hobson et al., 2017), which is present in high

418 pH solution as the vanadate oxyanion (VO_4^{3-}; Wehrli and Stumm (1989)). Thus, V

419 concentrations observed during BOF slag leaching are likely to be controlled by $Ca_3(VO_4)_2$

420 solubility limits ($K_{sp} = 10^{-17.97}$; Huijgen and Comans (2006), Cornelis et al. (2008), Allison et

421 al. (1991)) which impose an inverse relationship between Ca and V concentrations in the

422 leachate (Fig. 5).

423      $$3Ca^{2+} + 2VO_4^{3-} \rightleftharpoons Ca_3(VO_4)_2 \qquad \text{(Eqn. 6)}$$
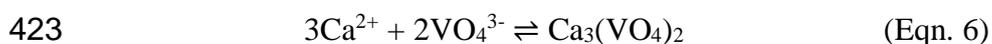
424   Under air-excluded conditions Ca released from CaO and dicalcium silicate weathering

425   accumulated in solution, producing a leachate with high Ca concentrations. The leachate

426   solution, therefore, quickly reached $Ca_3(VO_4)_2$ solubility limits, preventing further release of

427   V to solution and limiting V concentrations in the leachate.

428   Aerated conditions, however, allow in-gassing of atmospheric CO_2 and associated

429   formation of secondary carbonate minerals. This process provides a sink for Ca, lowering

430   aqueous Ca concentrations. The V that is released therefore persists in solution (due to the

431   lower $[Ca^{2+}].[VO_4^{3-}]$ ion activity product), leading to much higher concentrations than those

432   seen under air-excluded conditions. Monohydrocalcite is relatively soluble ($Ksp = 1 \times 10^{-7.1}$;

433   Kralj and Brečević (1995)), therefore, the equilibrium phase controlling Ca concentrations in

434   these experiments is probably dolomite ($CaMg(CO_3)_2$; $Ksp = 1 \times 10^{-17.2}$; Sherman and Barak

435   (2000)). Indeed, the predicted Ca concentration in solutions equilibrated with dolomite and

436   atmospheric pCO_2 are similar to those found at the end of these experiments (Fig 5; (Langmuir,

437   1997)). In the aerated experiments, the overall

438   [FIGURE 5]

439   leachate chemistry remains undersaturated with respect to $Ca_3(VO_4)_2$, which is consistent with

440   the observed depletion of the V-hosting dicalcium silicate phase by the end of the aerated

441   experiments.

442

443   4.6   Implications for waste management

444   Co-disposed wastes such as those used in this study are unattractive for reuse in

445   furnaces due to their highly variable composition making it difficult to control the steelmaking

446   processes. Furthermore, the presence of MgO makes their reuse in civil engineering

447   applications difficult, since periclase hydration to form brucite leads to significant volumetric

448   expansion and cracking. Given these problematic characteristics, combined steelmaking wastes

449   are generally stored in landfill. Over time, rainwater inevitably infiltrates and reacts with

450   landfilled waste to generate leachate. Therefore, the storage environment plays a key role in

451   establishing leachate composition. There is a key interaction between Ca concentrations and

452   the solution pH, which controlled by the equilibrium with the dominant Ca-phase present (i.e.

453   portlandite, Ca-Si-H or $CaCO_3$). The presence of CO_2 is a key factor in determining which

454   secondary Ca phases are present during leaching and also the degree to which the primary

455   dicalcium silicate was leached (therefore, indirectly affecting the release of trace metals such

456   as V).

457   Under air-excluded conditions, the leaching profile of the combined waste is similar to

458   that of BOF slag (Hobson et al., 2017, De Windt et al., 2011, Huijgen and Comans, 2006, Costa

459   et al., 2016). Rapid dissolution of Ca-bearing phases without in-gassing of CO_2 leads to a high

460   pH, $Ca(OH)_2$ dominated leachate. High Ca concentrations limit V release due to $Ca_3(VO_4)_2$

461   solubility limits. Consequently, water saturated environments with limited opportunity for CO_2

462   ingress will provide the safest environment for waste storage. Leachate could either be

463   recirculated (and reach equilibrium with $Ca(OH)_2$) or be removed and treated off site to lower

464   its pH and allow carbonation without triggering V release (Gomes et al., 2017). Under aerated

465   conditions, lower alkalinity and Ca concentrations allow much higher V concentrations to

466   accumulate in leachate, as well as allowing dissolution of MgO to form a $Mg(OH)_2$ dominated

467   leachate which favours the formation of monohydrocalcite and dolomite as secondary

468   carbonate phases. Leaching under aerated conditions rapidly produces leachate with V

469   concentrations in excess of acute toxicity thresholds (280 μg L^{-1}; Fig 5) and all experiments

470   display V concentrations higher than chronic toxicity thresholds (19 μg L^{-1}, Buchman, 2008).

471   New proposals for V exposure based on recent reviews of ecotoxicology data (Smit, 2012)

472   have suggested new water quality standards for V of 1.2 and 3.0 μg L^{-1} for chronic and acute

473   exposure respectively. Almost all slag leachates reported (Fig 5) would exceed these more

474   stringent limits, therefore, leachate generated from co-disposed steel making wastes would

475   require careful management (and treatment prior to discharge) to avoid the potential for

476   environmental harm.

477   Extrapolating from experimental results to field scale predictions must always be done

478   with caution. For example, these experiments were performed on crushed powder samples at

479   much lower solid to liquid ratios than would typically be found in a heap leaching scenario. It

480   is much more likely that during heap leaching (due to high solid : solution ratios present) free

481   lime and dicalcium silicate dissolution will control leachate quality resulting in higher Ca

482   concentrations (i.e. leachate saturated with respect to $Ca(OH)_2$) and therefore lower V

483   concentrations compared to those seen in experimental systems (indeed most real site leachates

484   commonly contain V at order of magnitude lower concentrations than found in laboratory

485   experiments; Fig 5). However, the experimental results indicate that although carbonation

486   reactions are helpful in reducing pH and alkalinity over time, the Ca concentrations produced

487   may allow higher V concentrations to accumulate in leachates over time. Therefore leachates

488   produced from co-disposed steelmaking wastes will likely require monitoring and secondary

489   treatments (e.g. by employing wetlands or cascade systems; Gomes et al., 2017) for decades

490   after their initial disposal.

5   Conclusions

The co-disposed waste investigated in this study was composed of BOF steelmaking slag containing dicalcium silicate, wüstite, dicalcium aluminoferrite and free lime; and refractory oxides comprising corundum, periclase, graphite and high temperature aluminosilicate. V was predominately associated with the dicalcium silicate and dicalcium aluminoferrite phases. During leaching, alkalinity was produced by dissolution of free lime and dicalcium silicate. Under air-excluded conditions high Ca concentrations and the inverse relationship between Ca and V concentrations imposed by $Ca_3(VO_4)_2$ solubility limits restricted V release to the leachate. Under aerated conditions in-gassing of CO_2 promoted carbonation reactions and secondary carbonate formation. Leachate pH and Ca concentrations were reduced and MgO hydration and dissolution was promoted leading to a switch from a Ca to an Mg dominated leachate and precipitation of monohydrocalcite and dolomite. V concentrations in leachate were higher under aerated conditions where formation of carbonate minerals provides a sink for aqueous Ca following in-gassing of CO_2. Under these conditions, the inverse relationship imposed by $Ca_3(VO_4)_2$ solubility limits allows higher concentrations of V to accumulate in leachate than those seen under air-excluded conditions. Therefore, when considering long-term leaching behaviour, it is important that risk assessments consider the expected in situ environmental chemistry of specific waste storage environments.

25

515 Leicester and Bob Knight at the University of Hull for XRF and additional ICP-OES

516 respectively.

517 **References**

518 **ALLISON, J. D., BROWN, D. S. & NOVO-GRADAC, K. J. 1991.**
519   **MINTEQA2/PRODEFA2, a geochemical assessment model for environmental**
520   **systems: version 3.0 user's manual, Environmental Research Laboratory, Office of**
521   **Research and Development, US Environmental Protection Agency.**

522 **BAYLESS, E. R. & SCHULZ, M. S. 2003. Mineral precipitation and dissolution at two**
523   **slag-disposal sites in northwestern Indiana, USA. Environmental Geology, 45, 252-**
524   **261.**

525 **BUCHMAN, M. F. 2008. NOAA Screening Quick Reference Tables. Office of Response**
526   **and Restoration Division, National Oceanic andAtmospheric Administration,**
527   **Washington, DC.**

528 **CHAURAND, P., ROSE, J., DOMAS, J. & BOTTERO, J. Y. 2006. Speciation of Cr and**
529   **V within BOF steel slag reused in road constructions. Journal of Geochemical**
530   **Exploration, 88, 10-14.**

531 **CHESTERS, J. H. 1973. Refractories: production and properties, Iron and Steel Institute.**

532 **CORNELIS, G., JOHNSON, C. A., GERVEN, T. V. & VANDECASTEELE, C. 2008.**
533   **Leaching mechanisms of oxyanionic metalloid and metal species in alkaline solid**
534   **wastes: A review. Applied Geochemistry, 23, 955-976.**

535 **COSTA, G., POLETTINI, A., POMI, R. & STRAMAZZO, A. 2016. Leaching modelling**
536   **of slurry-phase carbonated steel slag. Journal of Hazardous Materials, 302, 415-**
537   **425.**

538 **DANA, K. & DAS, S. K. 2004. Partial substitution of feldspar by B.F. slag in triaxial**
539   **porcelain: Phase and microstructural evolution. Journal of the European Ceramic**
540   **Society, 24, 3833-3839.**

541 **DE SA, R. G., E SILVA, G. L. & BITTTENCOURT, L. 2007. Recycling of spent**
542   **refractories from metallurgical processing management and technological**
543   **approach. 8th UNITECR, Dresden, Alemania.**

544 **DE WINDT, L., CHAURAND, P. & ROSE, J. 2011. Kinetics of steel slag leaching: Batch**
545   **tests and modeling. Waste Management, 31, 225-235.**

546 **ELONEVA, S., PUHELOINEN, E.-M., KANERVA, J., EKROOS, A., ZEVENHOVEN,**
547   **R. & FOGELHOLM, C.-J. 2010. Co-utilisation of CO2 and steelmaking slags for**
548   **production of pure CaCO3 – legislative issues. Journal of Cleaner Production, 18,**
549   **1833-1839.**

550 **ENVIRONMENT AGENCY 2014. EA Bespoke permit 2014 Permit for Scunthorpe**
551   **Aggregate processing. Permit number EPR/LP3537VV/A001.**

552 **GEISELER, J. 1996. Use of steelworks slag in Europe. Waste Management, 16, 59-63.**

GOMES, H. I., ROGERSON, M., BURKE, I. T., STEWART, D. I. & MAYES, W. M. 2017. Hydraulic and biotic impacts on neutralisation of high-pH waters. Science of The Total Environment, 601–602, 1271-1279.

HANAGIRI, S., MATSUI, T., SHIMPO, A., ASO, S., INUZUKA, T., MATSUDA, T., SAKAKI, S. & NAKAGAWA, H. 2008. Recent improvement of recycling technology for refractories. SHINNITTETSU GIHO, 388, 93.

HOBSON, A. J., STEWART, D. I., BRAY, A. W., MORTIMER, R. J. G., MAYES, W. M., ROGERSON, M. & BURKE, I. T. 2017. Mechanism of Vanadium Leaching During Surface Weathering of Basic Oxygen Furnace Steel Slag Blocks: A Microfocus X-ray Absorption Spectroscopy and Electron Microscopy Study. Environmental Science and Technology 51, 7823-7830.

HUIJGEN, W. J. J. & COMANS, R. N. J. 2006. Carbonation of steel slag for CO_2 sequestration: Leaching of products and reaction mechanisms. Environmental Science and Technology, 40, 2790-2796.

KRALJ, D. & BREČEVIĆ, L. 1995. Dissolution kinetics and solubility of calcium carbonate monohydrate. Colloids and Surfaces A: Physicochemical and Engineering Aspects, 96, 287-293.

KWONG, K. & BENNETT, J. 2002. Recycling Practices of Spent MgO-C Refractories. Journal of Minerals and Materials Characterization and Engineering, 1, 69-78.

LANGMUIR, D. 1997. Aqueous Environmental Geochemistry, Prentice Hall.

MATERN, K., RENNERT, T. & MANSFELDT, T. 2013. Molybdate adsorption from steel slag eluates by subsoils. Chemosphere, 93, 2108-2115.

MAYES, W. M. & YOUNGER, P. L. 2006. Buffering of Alkaline Steel Slag Leachate across a Natural Wetland. Environmental Science & Technology, 40, 1237-1243.

MAYES, W. M., YOUNGER, P. L. & AUMONIER, J. 2008. Hydrogeochemistry of alkaline steel slag leachates in the UK. Water Air and Soil Pollution, 195, 35-50.

MAZDIYASNI, K. S. & BROWN, L. M. 1972. Synthesis and Mechanical Properties of Stoichiometric Aluminum Silicate (Mullite). Journal of the American Ceramic Society, 55, 548-552.

NAVARRO, C., DIAZ, M. & VILLA-GARCIA, M. A. 2010. Physico-Chemical Characterization of Steel Slag. Study of its Behavior under Simulated Environmental Conditions. Environmental Science & Technology, 44, 5383-5388.

NIKOLIĆ, I., DRINČIĆ, A., DJUROVIĆ, D., KARANOVIĆ, L., RADMILOVIĆ, V. V. & RADMILOVIĆ, V. R. 2016. Kinetics of electric arc furnace slag leaching in alkaline solutions. Construction and Building Materials, 108, 1-9.

OBER, J. A. 2017. Mineral commodity summaries 2017. Mineral Commodity Summaries. Reston, VA.

PIATAK, N. M., PARSONS, M. B. & SEAL, R. R. 2014. Characteristics and environmental aspects of slag: A review. Applied Geochemistry.

POURBAIX, M. 1966. Atlas of electrochemical equilibria in aqueous solutions, Pergamon Press.

PROCTOR, D. M., FEHLING, K. A., SHAY, E. C., WITTENBORN, J. L., GREEN, J. J., AVENT, C., BIGHAM, R. D., CONNOLLY, M., LEE, B., SHEPKER, T. O. &

596   ZAK, M. A. 2000. Physical and chemical characteristics of blast furnace, basic
597   oxygen furnace, and electric arc furnace steel industry slags. Environmental
598   Science & Technology, 34, 1576-1582.

599 QUARANTA, N. E., CALIGARIS, M. G. & DÍAZ, O. Characterization of Converter
600   Refractories for Recycling. Materials Science Forum, 2014. Trans Tech Publ, 605-
601   610.

602 RILEY, A. L. & MAYES, W. M. 2015. Long-term evolution of highly alkaline steel slag
603   drainage waters. Environ Monit Assess, 187, 463.

604 ROADCAP, G. S., KELLY, W. R. & BETHKE, C. M. 2005. Geochemistry of extremely
605   alkaline (pH > 12) ground water in slag-fill aquifers. Ground Water, 43, 806-816.

606 RODRIGUEZ-BLANCO, J. D., SHAW, S., BOTS, P., RONCAL-HERRERO, T. &
607   BENNING, L. G. 2014. The role of Mg in the crystallization of monohydrocalcite.
608   Geochimica et Cosmochimica Acta, 127, 204-220.

609 ROVNUSHKIN, V. A., VISLOGUZOVA, E. A., SPIRIN, S. A., SHEKHOVTSOV, E. V.,
610   KROMM, V. V. & METELKIN, A. A. 2005. Composition of Ladle Slag and
611   Refractory Materials and Its Effect on the Wear Resistance of the Lining of an RH
612   Vacuum Degasser. Refractories and Industrial Ceramics, 46, 193-196.

613 SCHNEIDER, H., OKADA, K. & PASK, J. A. 1994. Mullite and mullite ceramics, J.
614   Wiley.

615 SHERMAN, L. A. & BARAK, P. 2000. Solubility and Dissolution Kinetics of Dolomite in
616   Ca–Mg–HCO3/CO3 Solutions at 25°C and 0.1 MPa Carbon Dioxide. Soil Science
617   Society of America Journal, 64, 1959-1968.

618 SHI, C. 2002. Characteristics and cementitious properties of ladle slag fines from steel
619   production. Cement and Concrete Research, 32, 459-462.

620 SHI, H., ZHAO, Y. & LI, W. 2002. Effects of temperature on the hydration
621   characteristics of free lime. Cement and Concrete Research, 32, 789-793.

622 SMIT C. E. 2012. Environmental risk limits for vanadium in water : A proposal for water
623   quality standards in accordance with the Water Framework Directive. RIVM Letter
624   Report 601714021/2012. National Institute for Public Health and the
625   Environment, Bilthoven.

626 STEWART, D. I., BRAY, A. W., UDOMA, G., HOBSON, A. J., MAYES, W. M.,
627   ROGERSON, M. & BURKE, I. T. 2018. Hydration of dicalcium silicate and
628   diffusion through neo-formed calcium-silicate-hydrates at weathered surfaces
629   control the long-term leaching behaviour of basic oxygen furnace (BOF)
630   steelmaking slag. Environmental Science and Pollution Research 25, 9861-9872.

631 TAMARI, N., KONDOH, I., TANAKA, T. & KATSUKI, H. 1993. Mechanical Properties
632   of Alumina-Mullite Whisker Composites. Journal of the Ceramic Society of Japan,
633   101, 721-724.

634 TAYLOR, H. F. W. 1986. Proposed Structure for Calcium Silicate Hydrate Gel. Journal
635   of the American Ceramic Society, 69, 464-467.

636 TOSSAVAINEN, M., ENGSTROM, F., YANG, Q., MENAD, N., LIDSTROM
637   LARSSON, M. & BJORKMAN, B. 2007. Characteristics of steel slag under
638   different cooling conditions. Waste Management, 27, 1335-1344.

639   **WALKER, C. S., SUTOU, S., ODA, C., MIHARA, M. & HONDA, A. 2016. Calcium**
640   **silicate hydrate (C-S-H) gel solubility data and a discrete solid phase model at**
641   **25°C based on two binary non-ideal solid solutions. Cement and Concrete**
642   **Research, 79, 1-30.**

643   **WEHRLI, B. & STUMM, W. 1989. VANADYL IN NATURAL-WATERS -**
644   **ADSORPTION AND HYDROLYSIS PROMOTE OXYGENATION. Geochimica**
645   **Et Cosmochimica Acta, 53, 69-77.**

646   **YI, H., XU, G., CHENG, H., WANG, J., WAN, Y. & CHEN, H. 2012. An Overview of**
647   **Utilization of Steel Slag. Procedia Environmental Sciences, 16, 791-801.**

648   **YILDIRIM, I. Z. & PREZZI, M. 2011. Chemical, Mineralogical, and Morphological**
649   **Properties of Steel Slag. Advances in Civil Engineering, 2011, 1-13.**

650   **ZHAO, L., LI, Y., ZHOU, Y. & CANG, D. 2014. Preparation of novel ceramics with high**
651   **CaO content from steel slag. Materials & Design, 64, 608-613.**
652

653 **Table 1**. Chemical composition of BOF steel slag samples from the Yarbrough Repository,
654 Scunthorpe UK, and the powder sample used in leaching tests.

Major Elements Nominal Oxide wt%	BOF slag (Hobson et al., 2017)	Powder sample (this study)
CaO	40 ±5	19 ±2
FeO	32 ±9	16 ±2
SiO_2	14 ±3	11 ±1
MgO	5.2 ±1	28 ±3
MnO	4.5 ±1	2.1 ±0.2
Al_2O_3	1.2 ±0.4	18 ±2
P_2O_5	1.3 ±0.4	0.87 ±0.09
V_2O_5	0.81 ±0.24	0.33 ±0.03
TiO_2	0.30 ±0.13	0.86 ±0.09
Cr_2O_3	0.24 ±0.13	3.3 ±0.3
SO_3	0.23 ±0.09	0.33 ±0.03
K_2O	n.d.	0.12 ±0.01
Na_2O	n.d.	0.18 ±0.02
SrO	n.d.	0.14 ±0.01
ZrO_2	0.02 ±0.01	0.14 ±0.01
BaO	n.d.	0.01 ±0.01
NiO	0.02 ±0.01	n.d.
CuO	0.01±0.01	n.d.
ZnO	n.d.	0.02 ±0.01
PbO	n.d.	0.03 ±0.01
LOI	n.d.	0.96
TOTAL	**98.9**	**100.9**

655
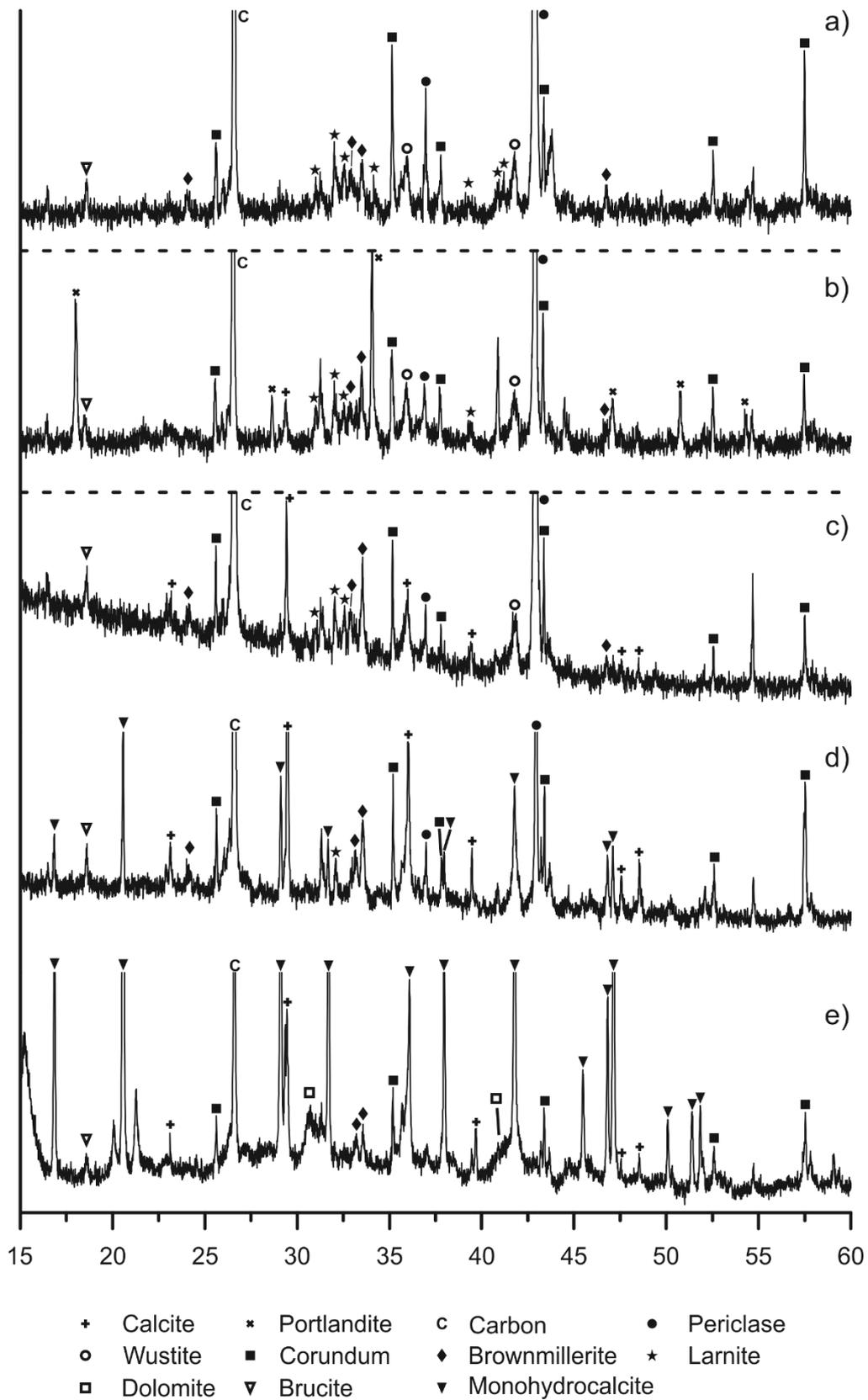
Figure 1. XRD patterns from (a) unweathered steelmaking waste, (b) steelmaking waste leached for 50 days under air-excluded conditions, and steelmaking waste leached under aerated conditions for (c) 1 hour, (d) 6 days and (e) 50 days
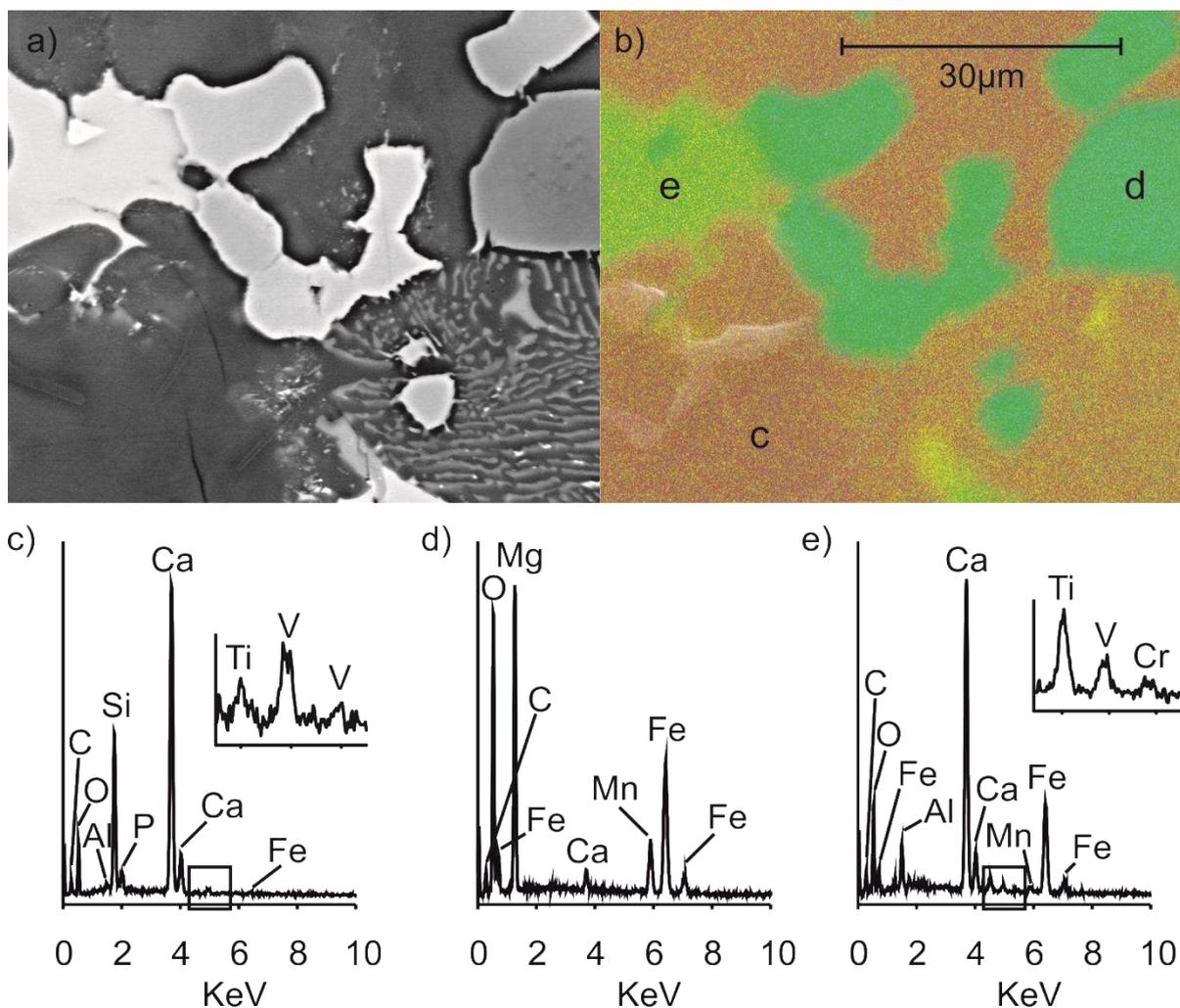
31

Figure 2. Backscattered electron micrograph (top left) with corresponding false colour element map (top right) and EDS spectra from c) dicalcium silicate, d) wüsite and e) dicalcium aluminoferrite phases. The laminae containing phase (bottom right) also contains discrete CaO laminae.

666
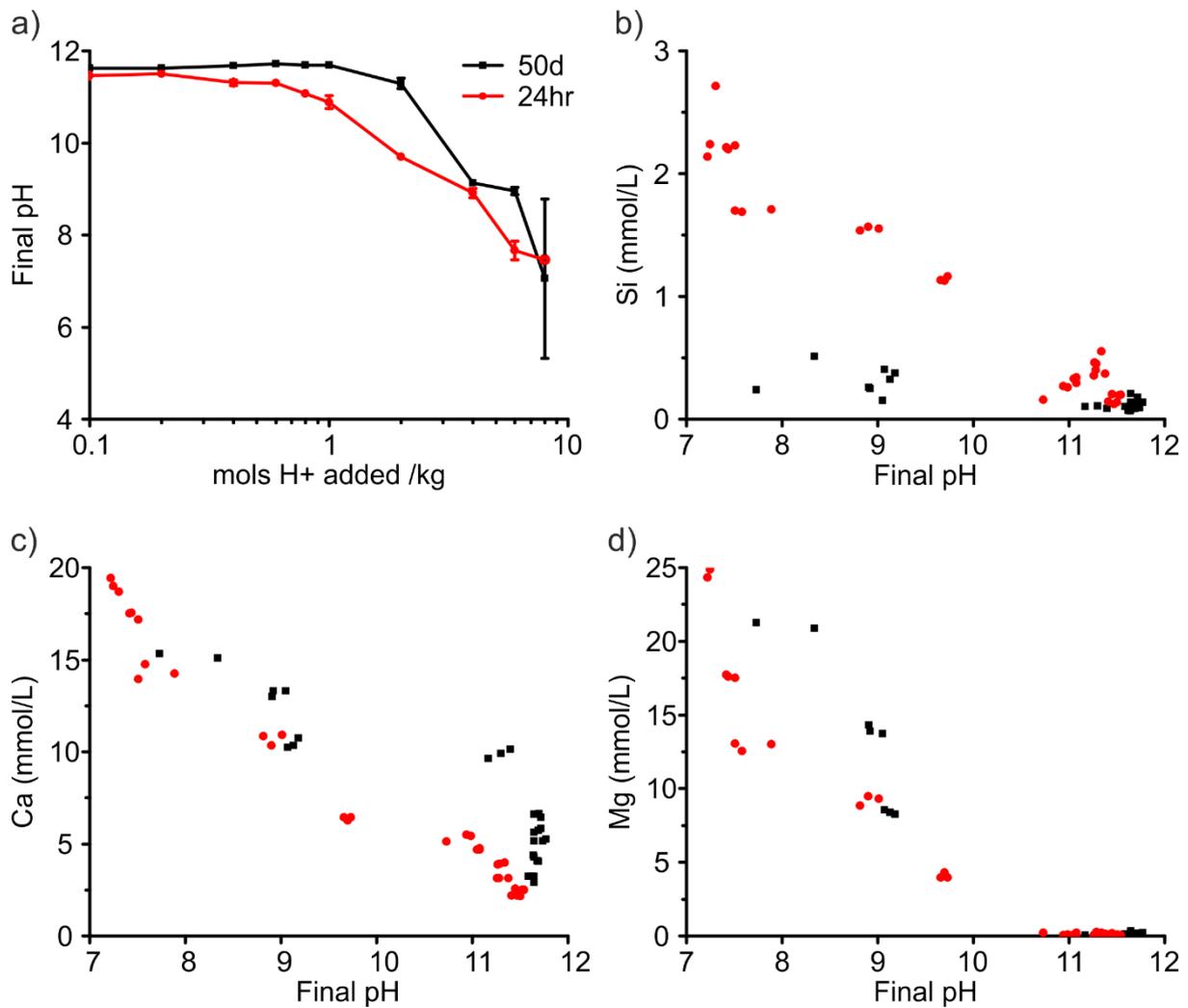
Fig. 3. Acid neutralisation results showing (a) final pH values after 24 hours (red circles) and 50 days (black squares) as a function of initial acid concentration (each point represents the mean value and error bars +/- 1σ from triplicate samples) and (b)-(d) metal concentrations leached from waste over 24 hours and 50 days as a function of final pH. Initial test conditions in all cases were 10g waste L^{-1}.
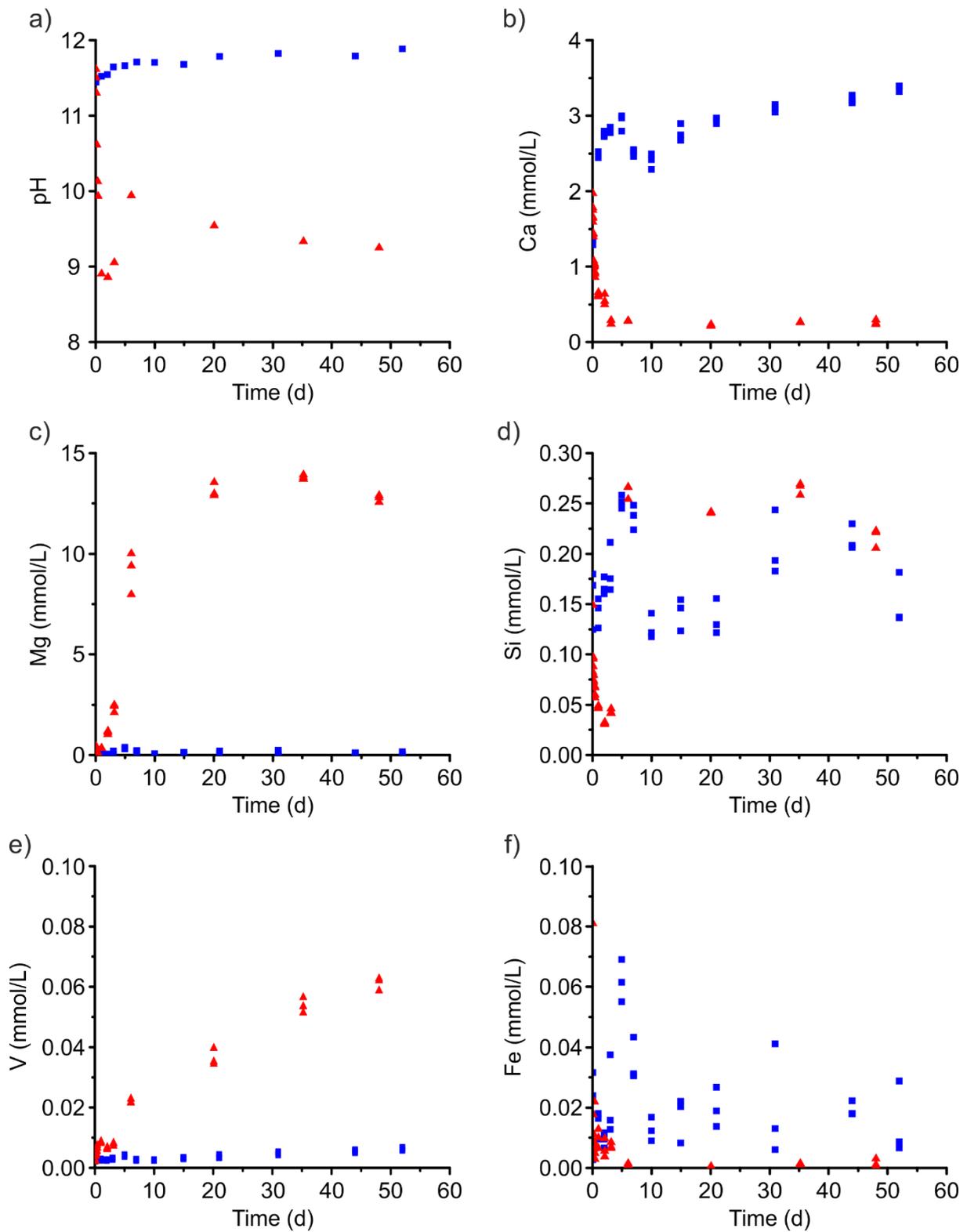
Figure 4. Leachate composition during the aerated (red triangle) and air-excluded (blue square) batch leaching test on steelmaking waste (initial test conditions: 10g solid/L deionised water). Data from triplicate experiments shown separately.

34
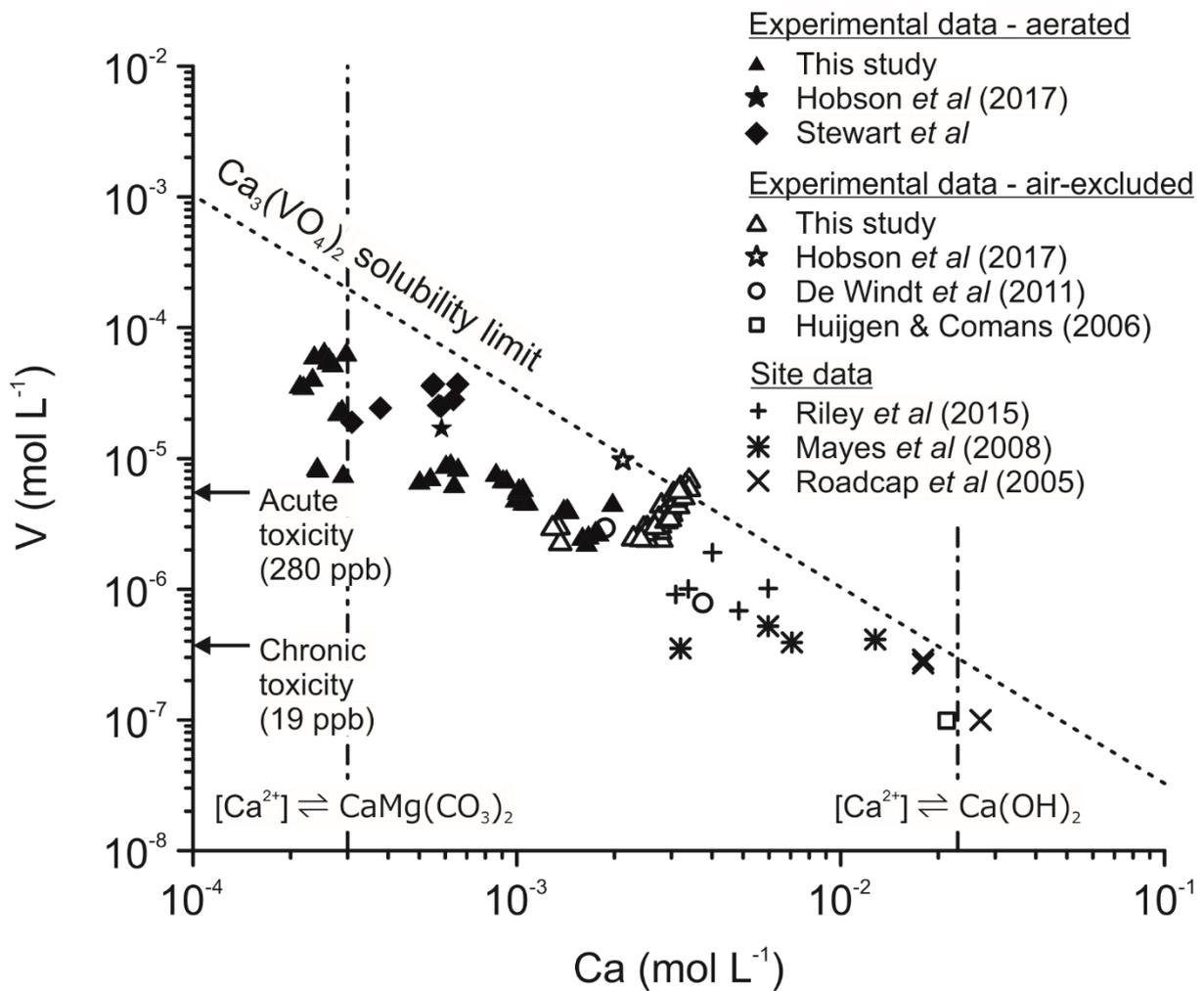
Figure 5. Plot of [V] versus [Ca] for selected experimental and site data (site data from Riley and Mayes (2015), Roadcap et al. (2005), Mayes et al. (2008)). The dashed line marks the solubility limits for $Ca_3(VO_4)_2$ at 20 °C (Allison et al., 1991). Data plotting below the solubility limit is undersaturated with respect to that phase. Vertical dashed lines indicate [Ca] in solutions in equilibrium with dolomite in contact with atmospheric CO_2, or with $Ca(OH)_2$, respectively (both at 20 °C). Horizontal arrows indicate acute and chronic freshwater toxicity guideline limits (Buchman, 2008) (Figure redrawn after Hobson et al. (2017)).